Article

Effect on Vehicle Turbocharger Exhaust Gas Energy Utilization for the Performance of Centrifugal Compressors under Plateau Conditions

Hong Zhang *, Hang Zhang and Zhuo Wang

School of Mechanical Engineering, Beijing Institute of Technology, Beijing 100081, China;
3120140221@bit.edu.cn (H.Z.); 2120150459@bit.edu.cn (Z.W.)

* Correspondence: zhanghong@bit.edu.cn; Tel.: +86-010-6891-1373

Abstract: This paper is focused on the performance of centrifugal compressors for vehicle turbochargers operating at high altitude. The reasons for turbocharged diesel engine power loss increases and bad economy performance caused by exhaust gas energy utilization are investigated. The atmosphere's impact on the turbocharger centrifugal compressor's energy distribution characteristics under the plateau is discussed. The key parameters that affect compressor characteristics are concluded in a theoretical method. A simulation calculation model is established to accurately predict compressor performance at high altitude. By comparing the experimental results, the calculation results are validated. The details of the internal flow fields analysis, including critical parameters of a compressor operating at high altitude, are analyzed. The results show that with the increase of altitude from 0 m to 4500 m, the peak efficiency of the compressor is reduced by 2.4%, while the peak pressure ratio is increased by 7%. The main influence characters of the plateau environment on the turbocharger centrifugal compressor performance, such as blade loads, exergy utilization and entropy distribution are concluded. The key factors for compressor performance and compressor energy flow control design method operated at high altitude are obtained.

Keywords: plateau conditions; vehicle turbocharger; centrifugal compressor

1. Introduction

Compared to plain areas, high plateau areas have characteristics such as low pressure, rarified air and a lack of oxygen, which can lead to some problems for vehicle engines: inadequate engine combustion, dropping power, and increased fuel consumption and emissions. There are some ways to recover the energy of a vehicle engine by reusing the waste gas energy [1], such as turbocharging [2], turbocompounding [3,4] or direct heat recovery [5]. Using new energy resources as electric vehicles to meet the needs of plateau application is also a solution, but the energy management and energy recover technology is still need to improve and develop [6–10]. Turbocharging technology (Figure 1), that can increase the output power of an internal combustion engine without the need to increase its cylinder capacity, which is superior for reducing the volume of the engine, has become a research hotspot. The turbocharging system can reuse the exhaust gas energy of the engine, which can provide energy to the compressor to compress inlet air, increasing the density of the engine intake, and compensating the intake energy for the engine, therefore promoting the combustion and increasing the engine power density, which is the main method to recover vehicle engine power in many fields.

In order to improve the matching performance of a turbocharged engine on the plateau, reference [11] matched a fixed turbocharger with a relief valve for a diesel engine, and the oil supply system was designed according to the plateau work demand, providing a supply system with altitude

compensation. Whole vehicle tests showed that the engine had good power and economy performance in the Tibetan Plateau and it can effectively avoid overheating and overspeeding of the turbocharger.

The plateau environment has a larger impact on the characteristics of the compressor which decides the performance of turbocharger. Usually, under plateau conditions, the compressor has insufficient charging pressure, it can easily surge, and the work temperature and speed will be higher. That will cause the problems of power decline and overspeeding of the compressor impeller. The study of gas energy utilization under plateau conditions to understand the flow characteristics and factors that influence the performance, play a decisive role in improving the plateau adaptability of the compressor, and further improving the matching state between turbocharger and the engine.
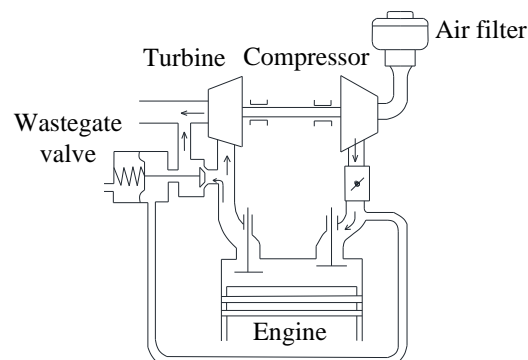

Figure 1. Principle of turbocharged engine.

Reynolds number is a critical factor that influences centrifugal compressor properties [12]. It is reduced a lot in a plateau environment. Wiesner [13] summarized the results of an investigation into the effects of Reynolds number on the performance of centrifugal compressor stages, using a computer program for the detailed prediction of components and overall performance characteristics. Strub [14] studied the influence of the Reynolds number on the performance of centrifugal compressors and obtained the influence mechanism through theoretical analysis. Feng [15] investigated the performance correction-transformation and analysis of plateau centrifugal compressors and found a correction method for the Reynolds number effects on the centrifugal compressor performance based on the equivalent pipe flow model. The quasi-similar characteristics of the compressor plateau and its conversion method are established, which provides practical means for matching calculation and road tests of plateau pressurization.

Xu et al. discussed the effects of the low Reynolds number on the turbine and compressor characteristics, analyzed the boundary trend of compressor gas flow that worked in a non-self-simulated domain with the increase of altitude, and deduced the correction formula of plateau turbocharging efficiency through similarity theory. Calibrated by the test data, the results can quickly estimate the plateau performance of the engine, and provide a theoretical basis for the influence of low Reynolds number on the performance of the engine [16].

With the development of numerical computation in recent years, the effects of Reynolds number on internal flow field of centrifugal compressor have studied through numerical analysis [17–19], which can greatly help us understand the flow and losses, such as the secondary flow mixing losses [20]. Through an experimental study of a centrifugal compressor, Johnson et al. [21] found that with the increase of the mass flow rate, the wake will be deflected to the pressure surface. Hirsch [22] summarized a high subsonic centrifugal compressor and the experimental and numerical simulation of centrifugal pump under low speed data, and the conclusion was that the position of the wake is the result of the equilibrium of a variety of secondary flow vortices and the tip leakage flow. Numerical simulation and theoretical analysis of three dimensional viscous flows in a low speed and large size centrifugal impeller were carried out by Kang [23], and the mechanism of jet wake structure was discussed in depth.

Wang et al. [24] numerically simulated the internal flow field of a transonic compressor under low Reynolds number conditions. The study found that a radial vortex flow exists in the flow boundary layer from the blade root to blade top in the compressor internal flow field. This vortex is caused by air separation of the transition zone of the boundary layer, and it can continuously develop and gather at the top of the blade. When the Reynolds number is further reduced under plateau conditions, a larger separation zone will be formed at the blade tip and becomes a key factor in causing the instability of compressor flow.

In summary, through the research on the effect of Reynolds number on the performance of the compressor by the experts, the conclusions can be drawn that when the Reynolds number is small at high altitude, the viscous force has a significant influence on the air properties, and the friction effect is relatively large, make air easy to separate [25]. Then the profile loss increases rapidly, the system pressure ratio and efficiency decline, and serious separation occurs, which will cause compressor rotation stalls and surges [26], which makes the engine performance degrade, and not work properly, which is one of the major current problems of engines working under a plateau environment.

Although numerical calculations have been carried out in the literature mentioned above, and the performance and flow field of compressors at low Reynolds number have been analyzed, a targeted analysis of the internal flow field in the vehicle turbocharger compressor operating at high altitude has not been carried out in the available literature. There are no detailed data on the internal energy loss of compressors in the plateau environment, especially the reasons why compressors operating in high altitude cause changes in the blade loads, exergy utilization and entropy distribution, etc. Therefore, in order to better understand the change characteristics of the compressor performance in a high altitude environment, improving the utilization of exhaust gas under plateau conditions, the compressor performance of a six cylinder turbocharged diesel engine is analyzed based on the theoretical analysis and numerical calculation, and compared with the experimental data. The Qinghai-Tibet Plateau in China is the world's highest plateau, with an average altitude of over 4000 m and many places that are over 4500 m. For most vehicles operating in the Tibet Plateau, 4500 m is a typical situation chosen as the studied and tested condition. Through three dimensional flow field analyses, the reasons for the performance change are clarified, which can provide a theoretical basis and strategies for compressor design under high altitude to meet the high altitude conditions of the vehicle turbocharger.

2. Compressor Performance Analysis

For the compressor, the compression medium types and attributes are the important factors that affect its performance. Under a plateau environment, the compressor inlet conditions change with altitude, and the plateau characteristics of the compressor can be expressed by Equation (1):

$$\pi_c, \eta_c = \mathrm{f}\left(M_c^*, n_c^*, C_p, K, P_r, Re \cdots\right) \tag{1}$$

The parameters in Formula (1) can be defined respectively by functions in Equations (2)–(6):

$$\pi_c = \frac{P_1}{P_0} \tag{2}$$

$$M_c^* = M_c \sqrt{T_0/298} \times 10^5 / P_0 \tag{3}$$

$$n_c^* = n_c \sqrt{298/T_0} \tag{4}$$

$$P_r = \frac{\mu C_P}{K} \tag{5}$$

$$Re = \frac{u_2 b_2 P_0}{\mu R T_0} \tag{6}$$

When the elevation increases from 0 m to 4500 m, the change rate of C_P in the physical properties is 0.2%, the change rate of the K value is 0.07%, the change rate of P_r is about 1%, and change rate of the three is very small. If we neglect the influence of the physical properties at the impeller inlet, Equation (1) can be expressed as:

$$\pi_c, \eta_c = f(M_c^*, n_c^*, Re) \tag{7}$$

In Equation (7), the dynamic viscosity coefficient model is given based on the Sutherland Model as follows:

$$\mu = \mu_0 \left(\frac{T}{273}\right)^{1.5} \left(\frac{273 + C}{T + C}\right) \tag{8}$$

For air, $\mu_0 = 1.711 \times 10^{-5}$ Pa·s, C = 122 K [27].

The circumferential velocity of the impeller can be expressed as:

$$u_2 = \frac{n_c \pi d_2}{60} \tag{9}$$

where d_2 is the impeller outlet diameter.

According to the definition of Reynolds number, the factors affecting it can be obtained by putting Equations (6), (8) and (9) into Equation (7):

$$
\begin{aligned}
Re &= \frac{u_2 b_2 P_0}{\mu R T_0} = \frac{n_c \pi d_2 b_2 P_0}{60 \mu_0 R T_0 \left(\frac{T_0}{273}\right)^{1.5} \left(\frac{273 + C}{T_0 + C}\right)} \\
&= \frac{n_c^* \pi d_2 b_2 P_0}{60 \times \sqrt{298 T_0} \mu_0 R \left(\frac{T_0}{273}\right)^{1.5} \left(\frac{273 + C}{T_0 + C}\right)} \\
&= k \left(\frac{P_0}{T_0} + \frac{P_0 C}{T_0^2}\right)
\end{aligned}
\tag{10}
$$

where k is the coefficient of the same rotational speed for the compressor. For the same compressor, the inlet temperature and the inlet pressure of the compressor decrease with the change of the environment under the plateau conditions. From Equation (10), it can be seen that at the same corrected speed, Reynolds number is only a function of the compressor inlet temperature and inlet pressure, and as the inlet temperature decreases, Reynolds number increases, and with the decreasing inlet pressure, Reynolds number decreases. Therefore, the low Reynolds number at the plateau is mainly due to the decrease of inlet pressure.

Under the plateau conditions, air density decreases rapidly, and the Reynolds number will also decrease. Air viscous force increases significantly under plateau conditions, so it is necessary to study the effects of the changing gas viscous force on the compressor performance. A turbocharger working at high altitude has another important feature: compared with the plain region, the turbine exhaust back pressure is low, the expansion ratio will increase, and the engine exhaust temperature is higher, so the output power of the turbine is higher than in the plain region, as the exhaust gas does more of the work in the turbine, which will lead to an automatic rise of the speed of the turbocharger and an increase of the pressure ratio, as is shown in Equation (11) [28]. As a result, the compressor has a higher pressure ratio than when working at high altitude. When the pressure ratio becomes higher, the compressor efficiency become lower, the turbocharger speed and charge air temperature are higher, as is shown in Equation (12). Small excess air coefficient and higher air inlet temperature, will improve the engine exhaust temperature, and the heat load of the engine and the turbine are increased:

$$W_T = m_e C_{pe} T_{03} \left(1 - \left(\frac{1}{\pi_T}\right)^{\frac{k-1}{k}}\right) \eta_T \tag{11}$$

$$\left(\pi_C^{\frac{k-1}{k}} - 1\right) = \left(1 - \frac{1}{\pi_T^{\frac{k-1}{k}}}\right)(1 + 1/AFR)\frac{C_{pe} T_{03}}{C_p T_{01}} \eta_{TC} \tag{12}$$

In order to compare the matching performance between compressor and engine at different altitudes, based on the experimental data, the engine operating curves overlayed on compressor characteristics curves on the plain and at 4500 m as shown in Figure 2. Under the plateau conditions, compared to the plain area, the load characteristic curve of the diesel engine will have an offset, and the risk of surge of the turbocharger increases. A turbocharger with a small surge mass flow rate is needed, a higher working speed must be allowable, the range of the mass flow rate must be wider and the adiabatic efficiency must be high when the pressure ratio is high. Therefore, in order to guarantee the full use of the exhaust gas energy under the plateau environment to restore the engine power, the turbocharger centrifugal compressor needs to be designed to keep the higher requirements for plateau application.
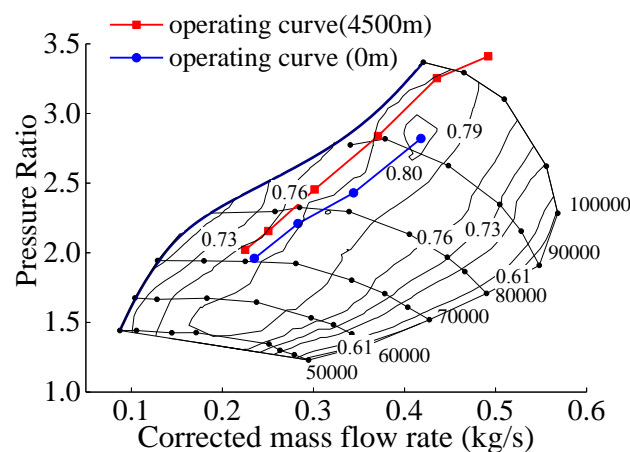

Figure 2. Compressor performance matching with engine operating curves.

3. Numerical Calculation Method

A numerical calculation model on a six-cylinder diesel engine turbocharger centrifugal compressor is built in the commercially available CFD code NUMECA (NUMECA International, Brussels, Belgium). The outlet diameter of the compressor impeller is 93 mm, the number of the main blades and the splitter blades are both 7. The ideal gas is selected as the medium, the Turbulent Navier-Stokes model [29] is applied as the mathematical model, and the turbulent model is the S-A equation model. The rotor-stator interface is using the circumferential conservation type junction surface. At the inlet boundary, the boundary condition is set as total temperature, total pressure and the flow direction is given. At the outlet boundary, uniform static pressure is given. The grid number for a single impeller is 0.93 million and the volute grid number is 1.1 million, respectively as shown in Figure 3. The y+ value of the first layer is less than 5, which satisfies the requirement of the turbulence model. In this paper, the numerical simulation mainly aims at the speed of 90,000 RPM at the altitude of 0 m and 4500 m. The specific parameters of the boundary conditions are listed in Table 1.

Table 1. Boundary conditions.

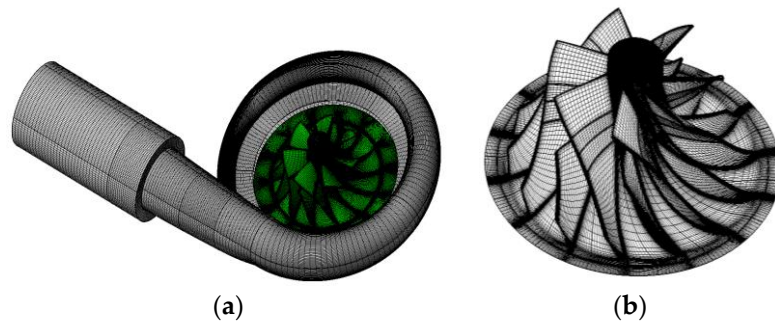| Altitude/m	Inlet Total Temperature/K	Inlet Total Pressure/kPa	Rotational Speed/rpm	Solid Wall
0	298	100	90,000	Adiabatic, no slip
4500	269	56	90,000	Adiabatic, no slip

Figure 3. Grid of the centrifugal compressor: (**a**) Compressor mesh; (**b**) Impeller mesh.

4. Calculation Results Analysis

4.1. Compressor Performance Comparison

In Figure 4 shows the pressure ratio and efficiency characteristics. The experimental data is obtained by a compressor test bench in a high altitude environment simulation cabin. Comparing the experimental and CFD results, the efficiency has 3.1% difference at most, and the pressure ratio has 3.3% difference at most in low flow rate. The differences are analyzed by test bench limited for accurate control of pressure and temperature. The trend of pressure ratio and efficiency are almost the same. From the CFD data, due to the increase of altitude from 0 m to 4500 m, the mass flow range of the compressor has a migration to the smaller mass flow rate zone as a whole. The results show that with the increase of altitude, the peak efficiency of the compressor is reduced by 2.4%, while the peak pressure ratio is increased by 7%. According to the previous theoretical analysis, the low temperature under a plateau environment leads to the compressor pressure ratio increase, while the lower Reynolds number is the main reason for the decline of the efficiency.
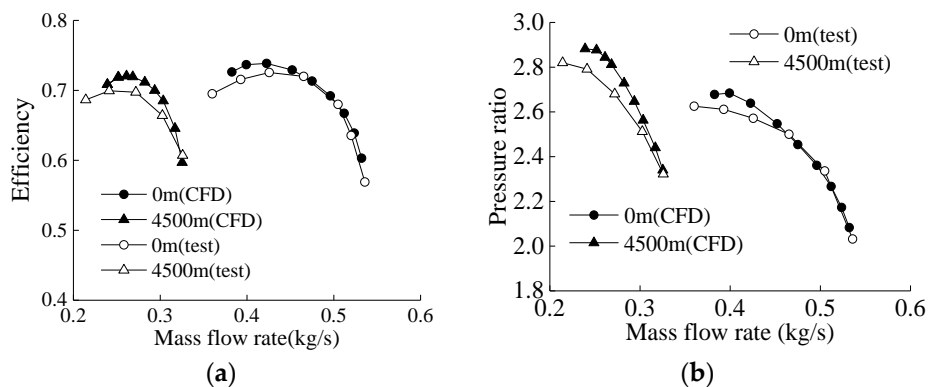

Figure 4. Change of compressor performances: (**a**) Efficiency characteristics; (**b**) Pressure ratio characteristics.

Figure 5 shows the relationship between the pressure ratio, the efficiency and the volumetric flow rate of the compressor. With increasing altitude, the inlet temperature and inlet pressure will decrease, the efficiency and the pressure ratio characteristics are basically the same, the efficiency, the peak pressure ratio of the compressor volume flow correspond to the basic agreement. Therefore, in different altitudes, although the compressor inlet conditions change, the characteristics of the compressor are similar, the main difference is the change of flow capacity of the compressor mass flow caused by the change of density.
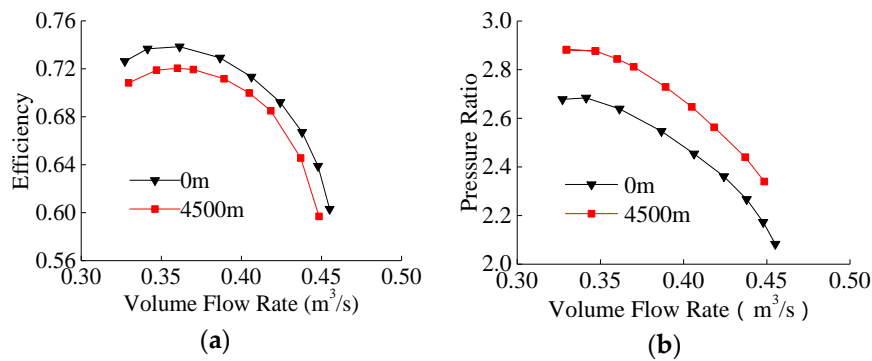
Figure 5. Characteristics of compressor volume flow rate, pressure ratio and efficiency: (**a**) Efficiency characteristics; (**b**) Pressure ratio characteristics.

4.2. Internal Flow Analysis in the Compressor

The efficiency peak points of the compressor at altitudes of 0 m and 4500 m are calculated, respectively. Figure 6 shows the relative Mach number distribution at the meridional averaged plane of the compressor. It can be seen that, as altitude increases, the compressor inlet temperature is reduced, the speed of sound declined, high-speed flow area near the impeller leading edge expands, which can lead to more shock losses. Figure 7 shows the relative Mach number distribution at the inlet of the impeller. It can be seen from the figure that, with increasing altitude, the range of supersonic area at impeller inlet obviously increases. When the supersonic airflow is disturbed by blade rotation, it is easy to produce shock waves, and lead to efficiency declination. The conclusion can be drawn that the shock loss increases with increasing altitude.
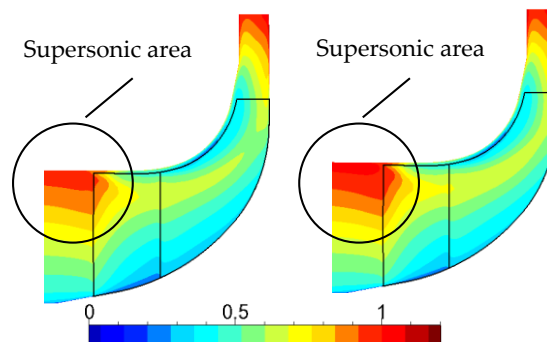

Figure 6. Relative Mach number distribution at the meridional averaged surface ((**left**) plain, (**right**) plateau).
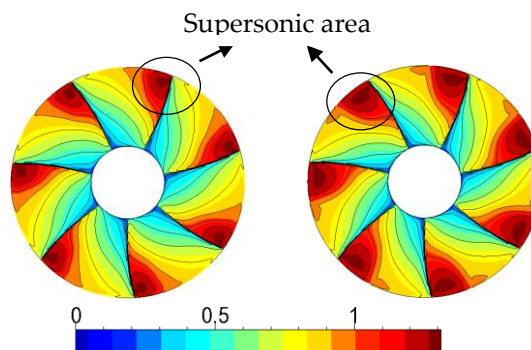

Figure 7. Relative Mach number distribution at the inlet of the impeller ((**left**) 0 m, (**right**) 4500 m).

Figure 8 shows the static pressure ratio distribution at the meridional averaged surface. Seen from the results, the meridional averaged static pressure ratio distributions in the compressor are similar, but as the altitude increases, the compressor impeller static pressure gradient increases, which leads to higher pressure ratio at the impeller outlet.
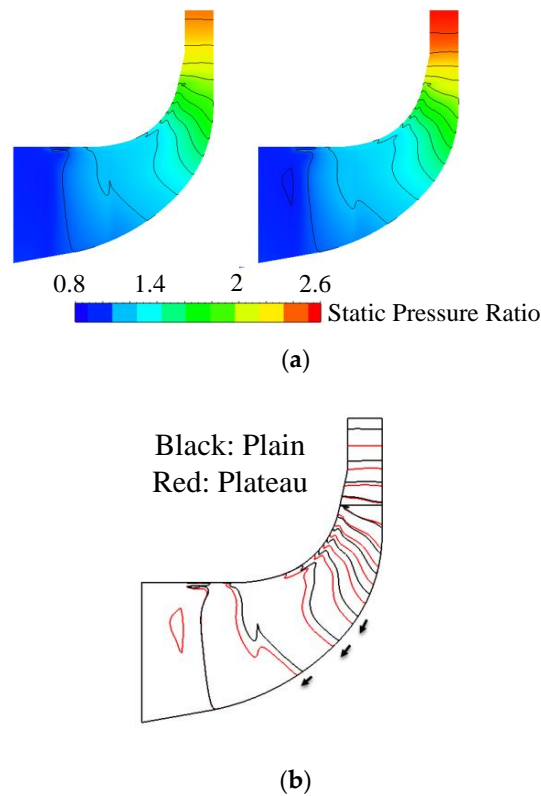

(**a**)

(**b**)

Figure 8. Static pressure ratio distribution on the meridional averaged surface: (**a**) (**left**) plain, (**right**) plateau; (**b**) contour lines superposition graph.

It can be seen from the contour lines superposition graph that the pressure gradient is obviously increasing at the downstream side, which leads to the contour lines becoming dense. Figure 9 is the entropy distribution of meridional averaged plane. According to the diagram, the high entropy area in the impeller is mainly distributed at the top of the blade and the outlet of the blade. It can be seen that with the inlet pressure and Reynolds number decreasing, the high entropy region of the blade top increases, and the loss increases.
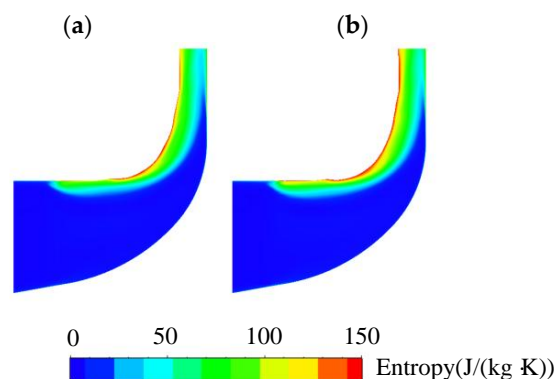

Figure 9. Entropy distribution of meridional averaged plane ((**a**): plain; (**b**): plateau).

Figure 10 show the distribution of the meridional averaged relative Mach number and static pressure along the flow direction on 50% blade span. In the figures points 1–3 are respectively the position at 13%, 41% and 70% of the blade arc length. The distribution shows that the relative Mach number declines from impeller inlet to impeller outlet, the static pressure ratio has a general upward trend. With increasing altitude, the relative Mach number along the flow direction has an overall upward trend, the difference becomes smaller from the position 3. Static pressure nearly remains the same before position 2, and it begins to rise from position 3. Due to the flow area at the leading edge of the main blade and the splitter blade becoming smaller, the distribution of relative Mach number shows two peaks at position 1 and position 2, and the distribution of static pressure shows two valleys. From position 3, the relative Mach number drops dramatically, and with increasing altitude, the falling gradient increases. Static pressure ratio has increased dramatically from position 3, too. Therefore, with the altitude increasing, compressor internal fluid kinetic energy transforms into pressure energy, which leads to more rising of the compressor pressure ratio.
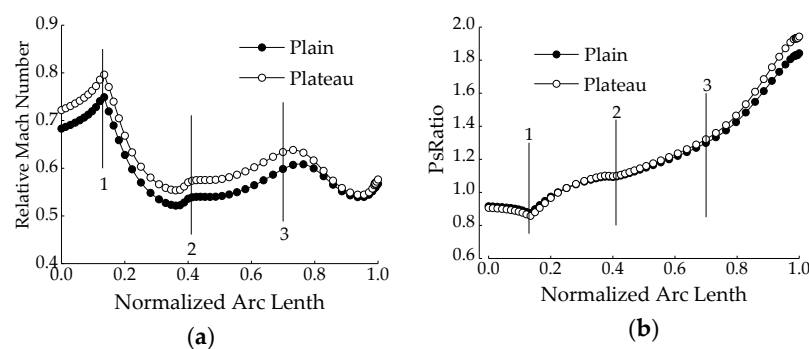

Figure 10. Distribution of relative Mach number and static pressure ratio along meridian direction: (**a**) Relative Mach number; (**b**) Static pressure ratio.

Figures 11–13 show the plain and plateau status from the blade surface load distribution of blade root to tip section. It can be seen that the blade surface load is gradually increasing along the flow direction on the whole. With the increasing altitude, the blade loads all appear enlarged a little. At the 10% blade span of the main blade, as shown in Figure 11, the load distribution starts to increase from about 60% position of the flow direction, and the starting position to increase gradually shift to the downstream when the blade span increases from 50% to 90%. The load variation reduces, too. For the splitter blade, the starting positions for load to increase at three blade span are all near 40% position of the flow direction and the load change are not noticeable as the main blade. For the suction side of the main blade, the load reduces near 20% of the flow direction, but the splitter blade doesn't change in the same position.
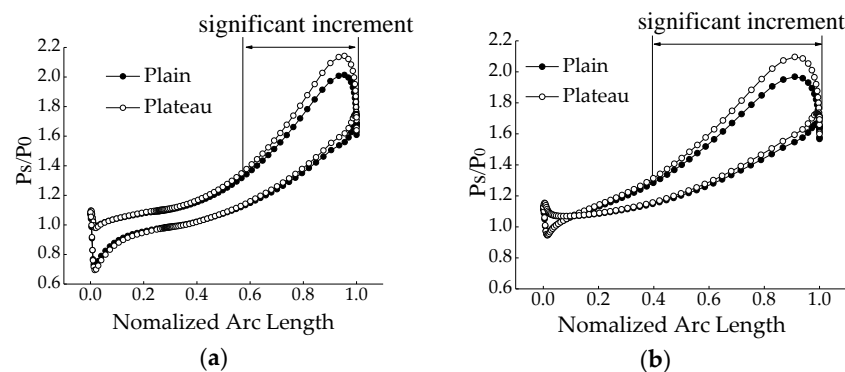

Figure 11. Load distribution of blade surface at 10% blade span: (**a**) main blade; (**b**) splitter blade.
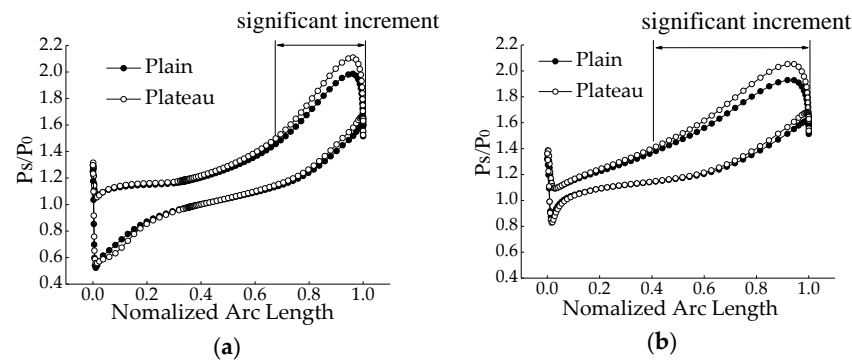
Figure 12. Load distribution of blade surface at 50% blade span: (**a**) main blade; (**b**) splitter blade.
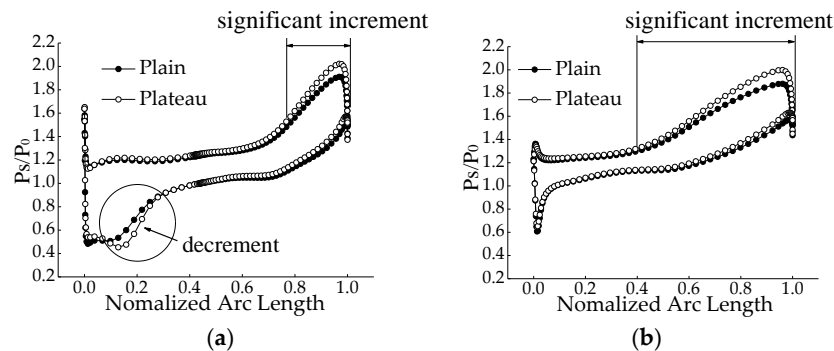

Figure 13. Load distribution of blade surface at 90% blade span: (**a**) main blade; (**b**) splitter blade.

According to the analysis above, the main blade load is more sensitive to the altitude, and has an obvious change at the downstream of the pressure side and upstream of the suction side. Because a load increment means the impeller will do more work with the air, which is beneficial to compensate for the reduction of the efficiency loss caused by the plateau flow loss, so it could be taken into consideration when designing compressor impellers for operating at high altitude.

As shown in Figure 14, the low speed zone in Figure 9a and the big gradient area in Figure 9b are mainly located at the leading edge of the splitter blade and the trailing edge part of the two blades. With the increasing altitude, the Reynolds number becomes lower, viscosity loss increases, the tip leakage flow movement becomes more intense, causing greater secondary flow losses at the leading edge of the splitter blade and the secondary flow losses at the two blades' trailing edge, the falling gradient increases, and the very low relative Mach number region becomes wider.
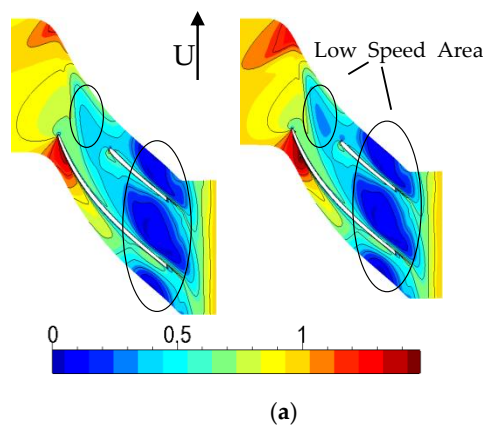

Figure 14. *Cont.*
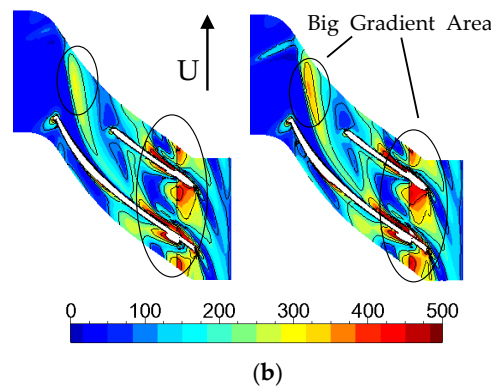
Figure 14. Distribution of the relative Mach number and its gradient at 90% blade span: (**a**) Relative Mach number ((**left**) plain; (**right**) plateau); (**b**) Distribution of the gradient of the relative Mach number ((**left**) plain; (**right**) plateau).

4.3. Exergy Destruction and Flow Loss Analysis in the Impeller

An exergy destruction, which is also called lost work, is the wasted work potential during a process as a result of irreversibility [30]. Irreversibility such as friction, mixing or non quasi-equilibrium compression always generates entropy and always destroys exergy. In order to analyze the exergy destruction happened at every parts of the compressor, as shown in Figure 10a, the compressor flow passage is divided into five paragraphs (a, b, c, d, e) through several key sections, for gas flow from inlet to either place "m" ("m" is any number from 1 to 5), the entropy increases can be calculated by the following equation:

$$\Delta \dot{S}_{rev(0-m)} = \int_{A_m} \left(C_p \ln \frac{T_m}{T_0} - R \ln \frac{p_m}{p_0} \right) \cdot \vec{v} \cdot d\vec{A}_m \tag{13}$$

When the gas flows from section "m" to section "n" ("n" is any number from 1 to 5), for an isolated system between these two sections, the entropy change is:

$$\Delta \dot{S}_{iso} = \Delta \dot{S}_{m-n} + \Delta \dot{S}_0 = \Delta \dot{S}_{rev(0-n)} - \Delta \dot{S}_{rev(0-m)}$$
$$= \int_{A_n} \left(C_p \ln \frac{T_n}{T_0} - R \ln \frac{p_n}{p_0} \right) \cdot \vec{v} \cdot d\vec{A}_n - \int_{A_m} \left(C_p \ln \frac{T_m}{T_0} - R \ln \frac{p_m}{p_0} \right) \cdot \vec{v} \cdot d\vec{A}_m \tag{14}$$

is the entropy increases of the environment, here the compressor surface is assumed adiabatic, only the internal flow loss is considered, so the entropy increase of the environment is zero. Eventually, the exergy destruction can be evaluated through the following equation:

$$\dot{I} = T_0 \Delta \dot{S}_{iso} \tag{15}$$

Based on the formulas above, as shown in Figure 15b, we can get the exergy destruction of every section of the compressor and the difference between plain and plateau, and it can be seen that at every section the loss is bigger on the plateau, because the Reynolds number decreases in the plateau environment, and the boundary layer become thick, thus the loss increases, but the loss at the impeller entrance "a" is small, and it only results in a slight increase under plateau condition. Compared to the plain area, the loss difference at section "b" is the biggest , and the loss difference at section "d" the second biggest, which shows that the impeller compressor energy loss increasing at section "b" and "d" is worsening, which is the important reason for the efficiency decline.

In order to study the reasons for the difference of exergy destruction, the flow of the gas is analyzed. For this four locations along the flow direction are selected: the leading edge of the main

blade, the leading edge of the splitter, the central line of the flow direction along the splitter blade, and the outlet of the impeller, and the changes of the flow angle at these locations are analyzed. It can be seen in Figure 16 that the difference between the flow angle on the plateau and plain is small, and even at location 3 the loss has a decrease [31], and this change means that the loss caused by the difference of flow angle is not the affecting factor. At the position 3, when the blade span is higher than 80% percent of the blade, the absolute value of the flow angle on the plateau is even smaller than the flow angle of the plain, which shows that the flow leakage doesn't increase. As is shown in Figure 17, there is an obvious high entropy area at 90% blade span, which is caused by the strong tip leakage flow. The entropy at the wake is higher at 50% and 10% blade span, and the high entropy wake area near the suction side of the splitter is stronger than the wake area near the main blade. The flow phenomenon above suggest that, with the increasing altitude, the Reynolds number reduces, the high entropy at the tip leakage flow area and the wake become greater, the loss get higher [32]. Because the flow leakage doesn't increase, the flow loss difference is mainly caused by the viscosity loss [33–35].
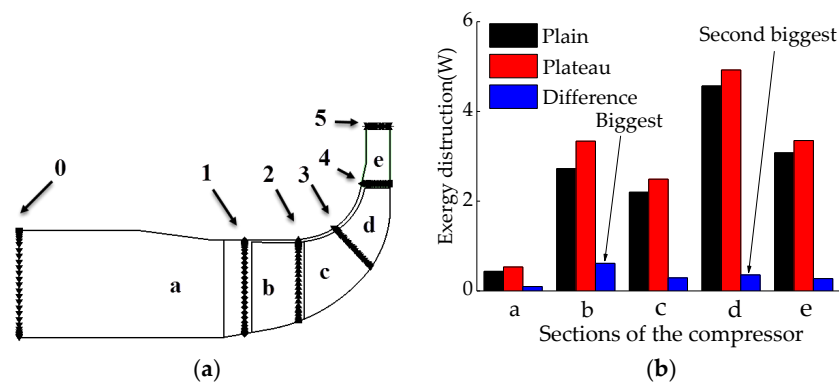

Figure 15. Exergy destruction comparison analysis: (**a**) Sections of the compressor passage; (**b**) Exergy destruction in the compressor.
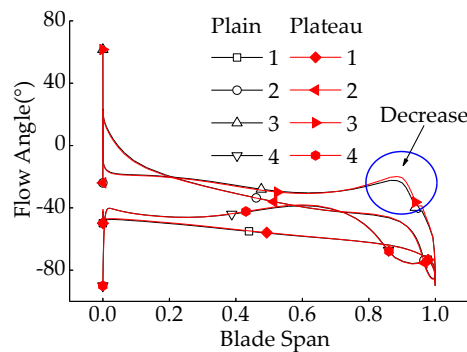

Figure 16. Distribution of flow angle at different impeller positions.

Figure 18 shows the relative meridional velocity and streamline distribution of the flow channel section at the blade tail. It can be seen that there is a large range of low velocity area at the side of the main blade (MB) and the splitter blade (SB) near the shroud surface. This is due to the presence of z strong viscous gas loss near the shroud, coupled with the impact of the adverse pressure gradient, leading to the gas speed near the shroud surface being far lower than the mainstream, forming a clear separation line, caused by leakage flow [36]. The leakage flow is mixing with the main flow in the flow channel, resulting in strong mixing loss and forming a low velocity zone near the casing. Figure 19 is the entropy distribution at the blade tail section. As can be seen from the diagram that the high entropy region is located at the low velocity region corresponding to Figure 18. It can be seen that with the decrease of inlet pressure, the Reynolds number decreases, the leakage flow intensifies, and

the high entropy region expands, which leads to greater mixing loss, which leads to the reduction of compressor efficiency.
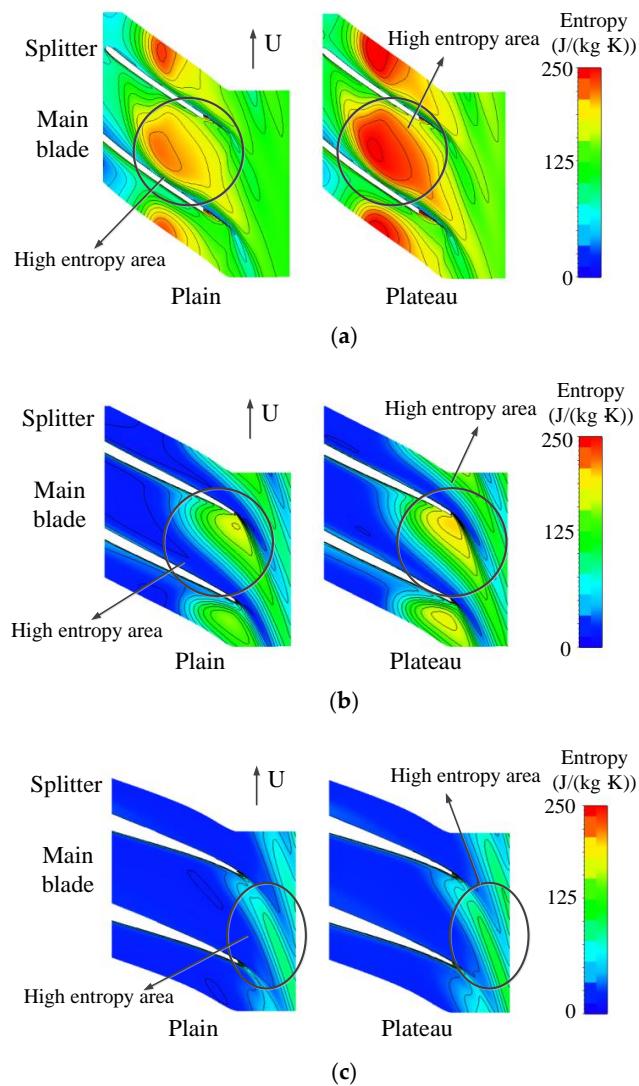

Figure 17. Entropy distribution of the impeller tail: (**a**) 90% blade span; (**b**) 50% blade span; (**c**) 10% blade span.
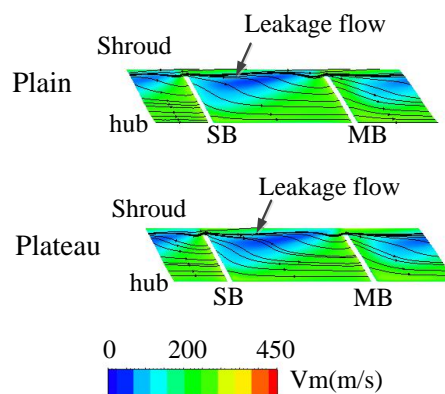

Figure 18. Relative meridional velocity and streamline distribution at channel section of the impeller trailing edge.
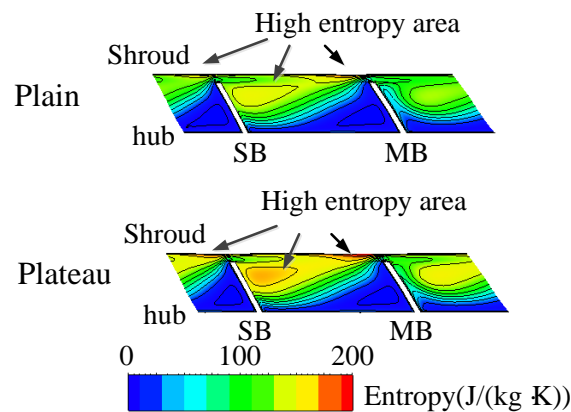
Figure 19. Entropy distribution at channel section of the impeller trailing edge.

4.4. Loss Analysis of Impeller Downstream

Figure 20 shows the entropy distribution of the 0-0 section of the volute under different inlet pressures. With the decrease of inlet pressure, the range of low entropy region in the volute is obviously reduced, and the range of high entropy region near the solid wall of the volute is obviously enlarged. With the decrease of pressure, the decrease of Reynolds number will lead to the increase of fluid viscosity and the thickening of boundary layer of solid wall, which will lead to the increase of flow loss. As shown in Figure 21, when the air flow into the volute, the pressure ratio increases, with the increase of the altitude, the static pressure ratio of the 0-0 section of the volute also increases. Figure 22 shows the distribution of the relative Mach number of the 0-0 section of the volute. It can be seen that the high relative Mach number zone is enlarged, which is mainly related to the decrease of the reverse pressure gradient of the compressor, but the change amplitude is less than static pressure.
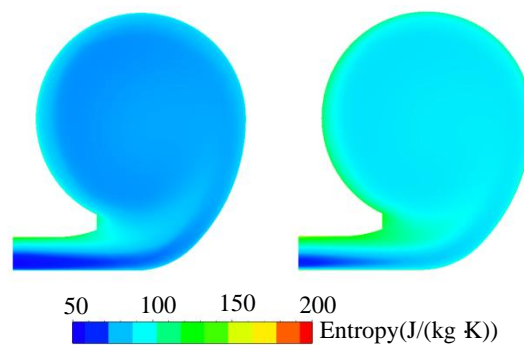

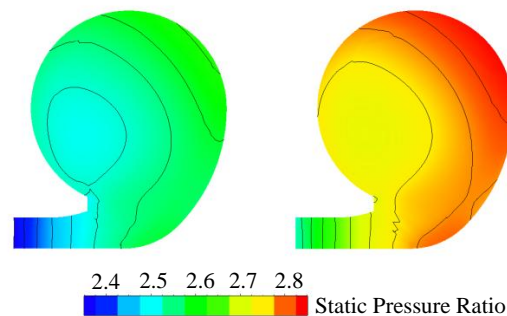**Figure 20.** Entropy distribution of 0-0 section of the volute ((**left**) plain, (**right**) plateau).

Figure 21. Distribution of static pressure ratio of 0-0 section of the volute ((**left**) plain, (**right**) plateau).
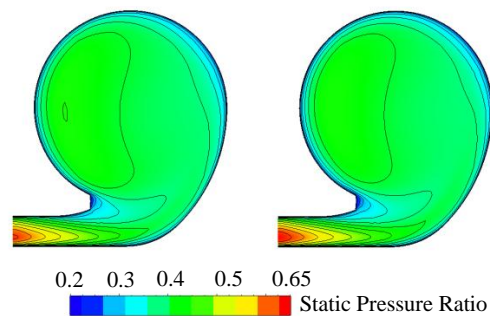
Figure 22. Distribution of relative Maher number of 0-0 section of the volute ((**left**) plain, (**right**) plateau).

Figure 23 is the entropy distribution on the section of the diffuser and volute. It can be seen that the high entropy region is mainly distributed at the intersection of diffuser and volute. With the increase of altitude, the Reynolds number decreases, the entropy value increases as a whole, and the inner part of the diffuser and the inner part of the volute generate more flow loss. Because the geometry of the volute tongue is the most special, the impeller outflow gas interference with volute tongue, resulting in greater losses.
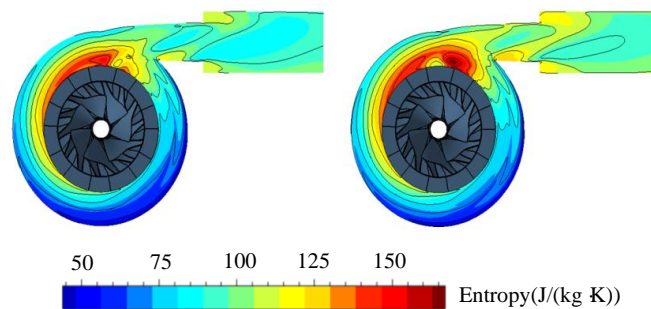

Figure 23. Entropy distribution on the section of diffuser and volute ((**left**) plain, (**right**) plateau).

5. Conclusions

When the turbocharger is working on a plateau, the performance is significantly decreased. In this paper, based on our theoretical analysis and numerical simulation calculation, the principles of change of compressor performance under high plateau conditions are concluded, the complicated internal flow field of a centrifugal compressor is analyzed, and the main impacts on the compressor performance degradation mechanism of the internal parameters are obtained. The key positions of energy loss are found on the basis of detailed compressor internal flow computation results. The design and optimization strategies for a compressor operating at high altitude are suggested. The following conclusions can be drawn:

(1) The high altitude work environment has remarkable effects on exhaust gas energy utilization for a vehicle turbocharger. The compressor inlet conditions change with altitude, which influences turbocharger compressor pressure ratio and efficiency features. The results show that with the increase of altitude from 0 m to 4500 m, the peak efficiency of the compressor is reduced by 2.4%, while the peak pressure ratio is increased by 7%. With the increase of altitude, the Reynolds number decreases and air viscous force increases significantly, which causes the efficiency of the compressor to drop obviously.

(2) From the detailed internal flow analysis in compressor, the main reasons for the low efficiency under the condition of the plateau environment include: the shock loss is increasing at the leading edge and the leakage flow loss is more intense at the downstream. The main blade load is more

sensitive to the altitude, and it has obvious change at the downstream of the pressure side and upstream of the suction side.

(3) The results show that, on the one hand, as the altitude increases, the compressor impeller static pressure gradient increases, the pressure contour lines will become dense, which can lead to higher pressure ratio at the impeller outlet, while on the other hand, blade loads all increase from 80% position of the main blade and 40% position of the splitter blade, which can contribute to the pressure ratio increment.

(4) The exergy destruction analysis shows that, with the increasing altitude, the leading edge of the impeller has the biggest exergy destruction difference, and the downstream of the compressor impeller passage has the second biggest exergy destruction difference, and more attention needs to be paid to these positions during compressor design.

(5) In the downstream of the impeller, due to the decrease of Reynolds number, the boundary layer is thickened, and the flow loss in the diffuser and volute is intensified, especially the position near the volute tongue. The region where the entropy is over 150 J/(kg·K) expands significantly near the volute tongue. These positions need a detailed optimization design to decrease flow losses and to satisfy the plateau condition requirements.

Author Contributions: Hong Zhang conceived and designed this study; Hang Zhang carried out the CFD computation and simulation; Hong Zhang performed the experiments; Hang Zhang and Zhuo Wang analyzed the CFD and experiments data; Hong Zhang and Hang Zhang wrote the paper.

Conflicts of Interest: The authors declare no conflict of interest.

Nomenclatures

Symbols

π_c	Compressor pressure ratio
η_c	Adiabatic efficiency
M_c^*	Corrected mass flow rate
n_c^*	Corrected rotational speed
C_p	Specific heat at constant pressure
K	Specific heat ratio
P_r	Prandtl number
Re	Reynolds number
M_c	Mass flow rate
n_c	Actual speed of the compressor
T_0	Inlet Total temperature
P_0	Inlet Total pressure
P_1	Outlet Total pressure
μ	Dynamic viscosity coefficient
u_2	Peripheral speed
b_2	Impeller blade outlet width
ρ_0	Air density at the impeller inlet
R	Gas constant of air
W_T	Output power of the turbine
m_e	Mass flow rate of gas
AFR	Air/Fuel Ratio
T_{03}	Turbine inlet temperature
T_{04}	Turbine outlet temperature
η_T	Efficiency of the turbine
η_{TC}	Efficiency of turbocharger
π_T	Expansion ratio of the turbine
C_{pe}	Gas specific heat at constant pressure

$\dot{S}$	Entropy of the airflow
p	Static pressure
$\Delta \dot{S}_0$	Entropy increases of the environment
$\dot{I}$	Exergy destruction

References

1. Saidur, R.; Rezaei, M.; Muzammil, W.K.; Hassan, M.H.; Paria, S.; Hasanuzzaman, M. Technologies to recover exhaust heat from internal combustion engines. *Renew. Sustain. Energy Rev.* **2012**, *6*, 5649–5659. [CrossRef]
2. Kusztelan, A.; Yao, Y.F.; Marchant, D.R.; Wang, Y. A Review of Novel Turbocharger Concepts for Enhancements in Energy Efficiency. *Int. J. Therm. Environ. Eng.* **2011**, *2*, 75–82. [CrossRef]
3. Mamat, A.M.I.; Romagnoli, A.; Martinez-Botas, R.F. Characterisation of a low pressure turbine for turbocompounding applications in a heavily downsized mild-hybrid gasoline engine. *Energy* **2014**, *64*, 3–16. [CrossRef]
4. Zhao, R.; Zhuge, W.; Zhang, Y.; Yang, M.; Martinez-Botas, R.; Yin, Y. Study of two-stage turbine characteristic and its influence on turbo-compound engine performance. *Energy Convers. Manag.* **2015**, *95*, 414–423. [CrossRef]
5. Zhao, M.; Xu, F.; Wei, M.S.; Tian, G.H.; Zhang, H. Simulation analysis of cooling methods of an on-board organic Rankine cycle exhaust heat recovery system. *Int. J. Energy Res.* **2017**. [CrossRef]
6. Zou, Y.; Liu, T.; Liu, D.; Sun, F. Reinforcement learning-based real-time energy management for a hybrid tracked vehicle. *Appl. Energy* **2016**, *171*, 372–382. [CrossRef]
7. Xiong, R.; Yu, Q.; Wang, L.Y.; Lin, C. A novel method to obtain the open circuit voltage for the state of charge of lithium ion batteries in electric vehicles by using H infinity filter. *Appl. Energy* **2017**, *207*, 346–353. [CrossRef]
8. Chen, C.; Xiong, R.; Shen, W. A lithium-ion battery-in-the-loop approach to test and validate multi-scale dual H infinity filters for state of charge and capacity estimation. *IEEE Trans. Power Electron.* **2018**, *33*, 332–342. [CrossRef]
9. Xiong, R.; Zhang, Y.; He, H.; Zhou, X.; Pecht, M.G. A double-scale, particle-filtering, energy state prediction algorithm for lithium-ion batteries. *IEEE Trans. Ind. Electron.* **2018**, *65*, 1526–1538. [CrossRef]
10. Xiong, R.; Tian, J.; Mu, H.; Wang, C. A systematic model-based degradation behavior recognition and health monitoring method for lithium-ion batteries. *Appl. Energy* **2017**, *207*, 372–383. [CrossRef]
11. Li, W.X.; Gao, W.Y.; Yuan, Z.Y.; Xing, X.C.; Wang, Y.Y.; Xu, X.Y. Study on Adaptability of CA6110/125Z1A2 Turbocharged Diesel Engine in Qing Zang Plateau. *Automob. Technol.* **2001**, *7*, 5–12.
12. Chen, F.; Wang, Y.F.; Chen, H.L.; Li, G.Z. Effects of Reynolds Number on Internal Flow Field of Centrifugal Compressor with the Volute. *J. Propuls. Technol.* **2013**, *7*, 911–917.
13. Wiesner, F.J. A New Appraisal of Reynolds Number Effects on Centrifugal Compressor Performance. *ASME J. Eng. Power* **1979**, *101*, 384–396. [CrossRef]
14. Strub, R.A.; Bonciani, L.; Borer, C.L.; Casey, M.V.; Cole, S.L. Influence of the Reynolds number on the performance of centrifugal compressors. *ASME J. Turbomach.* **1987**, *109*, 541–544. [CrossRef]
15. Feng, Z.P.; Shen, Z.D.; Zhao, J.B. Performance Correction-transformation and Analysis of Plateau Vehicle Turbochager Centrifugal Compressors. *Trans. CSICE* **1992**, *10*, 129–134.
16. Xu, B.; Bo, D.; Yao, H. Correction calculation for efficiency of the turbocharger of the plateau engine. *Veh. Eng.* **2009**, *6*, 7–10.
17. Huo, L.; Liu, H.X. Numerical analysis of centrifugal compressor performance and flow at low Reynolds number. *J. Air Power* **2013**, *28*, 911–920.
18. Sun, Z. Investigation on the Flow Features and Flowfield Structures of Centrifugal Compressor. Ph.D. Thesis, Institute of Engineering Thermophysics, Chinese Academy of Sciences, Beijing, China, 2011.
19. Wu, G.; Zhang, H.; Wei, M.S. Numerical Calculation and Analysis of the Plateau Characteristics of Centrifugal Compressor. *Veh. Power Technol.* **2014**, *4*, 1–5.
20. Hirsch, C.; Kang, S.; Pointet, G. A Numerically Supported Investigation of the 3D Flow in Centrifugal Impellers. Part II: Secondary Flow Structure. In Proceedings of the ASME Turbo Expo: Power for Land, Sea, and Air, Birmingham, UK, 10–13 June 1996.

21. Johnson, M.W.; Moore, J. Secondary Flow Mixing Losses in a Centrifugal Impeller. *ASME J. Eng. Power* **1983**, *105*, 24–32. [CrossRef]

22. Hirsch, C.; Kang, S.; Pointet, G. A Numerically Supported Investigation on the 3D Flow in Centrifugal Impellers. Part I: The Validation Base. In Proceedings of the ASME 1996 International Gas Turbine and Aeroengine Congress and Exhibition, Birmingham, UK, 10–13 June 1996.

23. Kang, S.; Hirsch, C. Numerical Simulation and Theoretical Analysis of the 3D Viscous Flow in Centrifugal Impellers. *J. TASK Q.* **2001**, *5*, 433–458.

24. Wang, R.G.; Zhou, M.; Zhao, Y.W.; Xia, Q.B.; Zeng, L.J. Research on flow instability mechanism of transonic compressor at low Reynolds number. *J. Aerosp. Power* **2009**, *24*, 414–419.

25. Liang, D.W.; Qian, H.J. Experimental investigation of aerodynamic characteristics of porous plates and numerical simulation of boundary layer suction. *Acta Aeronaut. Astronaut. Sin.* **2002**, *23*, 512–516.

26. Zhao, G.; Cai, Y.H.; Tu, Q.Y.; Wang, Z.X. Technological analysis for the turbofan engine of high altitude long endurance unmanned aerial vehicles. *J. Propuls. Technol.* **2009**, *30*, 154–158.

27. Zhu, D.X. *Turbocharging and Turbocharge*, 1st ed.; China Machine Press: Beijing, China, 1992.

28. Nicholas, C.B. *Fundamentals of Turbocharging*; Concepts ETI, Inc.: White River Junction, VT, USA, 2005.

29. Xia, Q.B.; Wang, R.G.; Li, Y.; Guo, F.F. Investigation on flow instability of transonic compressor rotor and the effects of CGCT on stall margin at low Reynolds number. *J. Propuls. Technol.* **2010**, *31*, 340–344.

30. Yunus, A.; Boles, M.A. *Thermodynamics: An Engineering Approach*; McGraw-Hill Series in Mechanical Engineering; McGraw-Hill Higher Education: Columbus, OH, USA, 2006; Volume 5.

31. Guo, Q.; Zhu, X.C.; Du, Z.H.; Chen, H.; Zhao, Y. Three-dimensional numerical simulation for rotating stall inside high-speed centrifugal compressor. *J. Propuls. Technol.* **2007**, *28*, 373–377.

32. Li, S.; Liu, C.; Hu, L.F.; Xing, W.D.; Yang, Z.H. Experimental Investigation on Centrifugal Compressor Performance Characteristics of Plateau Environment for Vehicle Turbocharger. *J. Mech. Eng.* **2016**, *20*, 151–158. [CrossRef]

33. Zhou, G.M.; Liu, R.L.; Dong, S.R.; Xiang, X.U.; Liu, G. A review of research on diesel engine plateau environment adaptability. *Veh. Eng.* **2013**, *207*, 1–5.

34. Zhao, Y.P. Review on Plateau Environment Adaptability of Diesel Engine. Ph.D. Thesis, Dalian University of Technology, Dalian, China, 2008.

35. Wang, Y.; Lin, F.; Nie, C.; Engeda, A. Design and Performance Evaluation of a Very Low Flow Coefficient Centrifugal Compressor. *Int. J. Rotat. Mach.* **2013**, *4*. [CrossRef]

36. Guidotti, E.; Toni, L.; Rubino, D.T.; Tapinassi, L.; Naldi, G.; Satish, K.; Prasad, S. Influence of Cavity Flows Modeling on Centrifugal Compressor Stages Performance Prediction Across Different Flow Coefficient Impellers. In Proceedings of the ASME Turbo Expo 2014: Turbine Technical Conference and Exposition, Düsseldorf, Germany, 16–20 June 2014.